Disc Fluttering in Stratified Flows

Try Lam, Lionel Vincent and Eva Kanso†

Department of Aerospace and Mechanical Engineering, University of Southern California, Los Angeles, CA 90089, USA

(Received xx; revised xx; accepted xx)

Stably stratified environments are found throughout nature in lakes, ponds, oceans, and the atmosphere. They are an important consideration in the analyses of falling debris and in the design of engineered autonomous vehicles and unpowered robots for space and ocean exploration because the fluid density variations may influence their motion. Here we investigate the settling of heavy discs in stably stratified salt water and compare their motion to that in constant density water. More specifically, we focus our investigation on fluttering descents, where the disc librates as it descends. We record the final landing location for multiple descents and compute the landing probability distribution function (*pdf*) in water and stratified flow. We also reconstruct the descent trajectories and orientations of the freely-falling discs. We find that stratification enhances the radial dispersion of the disc ($\sigma_s/\sigma_w \approx 2$), i.e., the *pdf* is more spread-out in the stratified environment, while simultaneously decreasing the vertical descent speed, fluttering amplitude, and the inclination angle during the descent. These findings may have significant impact on the understanding of unpowered robotic descents, and geological and biological transport where density and temperature variations may occur.

Key words: fluttering motion, stratified flow, free-falling motion [placeholder for entry; remove before submitting]

1. Introduction

Stably stratified fluids can found throughout nature in lakes, ponds, oceans, the atmosphere, and even in the sun. As an example, apart from the upper layer and isolated regions, the ocean is generally stably stratified, where the vertical density gradient is negative ($\gamma = d\rho/dz < 0$, where ρ is the density of the fluid and z is the vertical direction), or for the case of temperature stratification, a positive vertical temperature gradient. This is prevalent in isolated environments such as pores and fractures where mixing is negligible (MacIntyre *et al.* 2014), and intense biological activities and accumulation of particles and organisms were observed in stably stratified fluid.

In engineering, stable stratification can be utilized for heat and mass transports problems, such as cooling of nuclear reactor (Zhao & Peterson 2010) and energy generation from solar ponds (Lin 1982). In addition, stratification plays an important role in engineering design and analyses as density variations in the fluid may have unforeseen influences on an object's motion. A notable example, is the phenomenon known as "dead-water" phenomenon (Maas & van Haren 2006), where a boat on the surface experienced an increase in drag due to low pressure build up behind the vehicle from internal waves being generated along the interfaces of two-layer stratified fluid (Mercier *et al.* 2011),

† Email address for correspondence: kanso@usc.edu

such that the boat remains "dead" in the water. This phenomenon exist when a layer of lower density fluid, such as fresh water, overlays higher density fluid, such as sea water, e.g., at the mouth of a river or near melting glaciers. When testing swimmers, Ganzevles *et al.* (2009) found that strokes in stratified flow are less efficient and swim speed are much slower, by as much as 15%.

Similarly, enhanced drag was observed for horizontally moving spheres by Lofquist & Purtell (1984), and found that changes in the drag coefficient ΔC_D is a function of stratification level. Although many previous studies investigated horizontal motion in stratified flows, similar behaviors have been observed for flows in vertical motion (see Torres *et al.* 1999; Yick *et al.* 2009; Doostmohammadi *et al.* 2014), where an object's vertical motion is altered due to stratification. For example, for a linear stably-stratified flow for Re between 25-100, Torres *et al.* (1999) found an increase in the drag of a settling sphere is due to a rear buoyant jet forming behind the sphere.

For stratified flow without shear, the dynamics then depend on both Reynolds number $\mathrm{Re} = Ud/\nu$ and Froude number $\mathrm{Fr} = U/Nd$, where $N = (-\gamma g/\rho_0)^{1/2}$ is the Brunt-Väisälä (stratification) frequency, or the natural frequency of oscillation of a vertically displaced fluid parcel in the stratified fluid, ρ_0 is a reference density, γ is the density gradient of the fluid, ν is kinematic viscosity, d is diameter of the disc, U is the mean vertical velocity ($U = h/T$), h is the descent height, and T is the total time of the descent. The Froude number tells us about the stability and strength of the stratification. For strong stable stratification, the Froude number is a small real number. For the case of no stratification, e.g. pure water, $\mathrm{Fr} = \infty$. If shear forces are important, the Reynolds number Re and Froude number Fr can be combined and expressed in terms of the viscous Richardson number $\mathrm{Ri} = \mathrm{Re}/\mathrm{Fr}^2$, which express the relative importance of the stabilizing effect from buoyancy to the destabilizing shear forces. Note, this Richardson number is not the same as the one used in oceanography, which is used for large-scale vertical shear of water column. Here, the relevant shear forces originate from the descending object.

In this paper, we experimentally investigate the motion of fluttering discs in vertically stratified salt-water fluid and compare the motion to that of pure water. Even without the presences of stratification, such motion is rich in dynamics with complex interaction between the fluid and solid. Such unsteady free falling behaviors has attracted the attention of scientists as early as 1853 with Maxwell as he observed a rectangular slip of paper falling through the air (Maxwell 1990). Throughout the years, the falling patterns and associated phase space of discs falling in constant density fluid has been progressively refined for both numerical and experimental studies, and found that for small thickness-to-width ratio the falling patterns depends on the Reynolds number, Re, and the dimensionless moment of inertia, I^*. Notably, Willmarth *et al.* (1964) constructed a phase diagram by experimentally dropping disks with various thickness-to-diameter ratio. They were able to define a clear boundary in the phase space between steady and unsteady (fluttering and tumbling) oscillating motion. For $\mathrm{Re} < 100$, viscous forces dominate and a disc motion released with near zero initial conditions will descend steadily with small to no libration, regardless of I^*. For larger values of Re, when inertial forces plays a more dominant role, three other descent modes can be observed for difference ranges of I^*, as noted in Field *et al.* (1997). Stringham *et al.* (1969) perform similar experiments with spheres, cylinders, and disks and computed drag coefficients for a wide range of Reynolds numbers. Field *et al.* (1997) also experimented with varying initial release angles (disk's normal to the vertical) and found that the final angle is a function of the initial angle. See Ern *et al.* (2012) for a comprehensive review of both experimental and computational techniques of free-falling bodies in fluids. In general, the descent motion falls into four main types: steady, fluttering, tumbling, or chaotic depending on

Re and I^*, where the dimensionless moment of inertia $I^* = I/\rho_f d^5 = \pi\rho t/64\rho_f d$, where ρ is the density of the disc, and ρ_f is the density of the fluid.

Recently, Auguste *et al.* (2013) numerically explored similar falling motion of discs with parameter space in I^* and Archimedes number $Ar = \sqrt{3/32}U_g d/\nu$, which is a modified Reynolds number with gravitational speed $U_g = \sqrt{2|\rho/\rho_f - 1|gh}$. In their study, they explored Re < 300 (or approximately $Ar < 110$), and defined additional non-planar sub-regimes they referred to as hula-hoop (gyrating while fluttering) and helical autorotation (tumbling with plane rotation). The hula-hoop behavior is also observed in Heisinger *et al.* (2014). This zigzag or fluttering motion was also experimentally investigate by Zhong *et al.* (2013) where they used dye visualization and particle image velocimetry (PIV) to understand the flow structure of fluttering motion for different disc thickness-to-diameter ratios. Lee *et al.* (2013) expanded the experiment by looking at transitions from two-dimensional fluttering to spiral motions, and noted a critical Reynolds number where the transition occurs. They also looked at different initial release angles and how it influences the fluttering trajectories.

Numerical investigations were also conducted by Jin & Xu (2008), Pesavento & Wang (2004), Andersen *et al.* (2005*a*), Andersen *et al.* (2005*b*), and Chrust *et al.* (2013) for thin discs and cards. Jin & Xu (2008) developed a moving mesh method for Navier-Stokes equations and had good agreements between experimental and computational trajectories, and clarified some discrepancies noted in Andersen *et al.* (2005*b*), who along with Andersen *et al.* (2005*a*) and Andersen *et al.* (2005*b*) studied the free falling dynamics in a quasi-steady force model in the body frame. Similar to Auguste *et al.* (2013), Chrust *et al.* (2013) numerically studied the dynamics of free falling disc, but parameterize the phase space using the non-dimensionalized mass $m^* = m/\rho_f d^3$ and the Galileo number $G = \sqrt{|m^* - (V/d^3)|gd^3}/\nu$, where V is the volume of the body. The Archimedes number is related to the Galileo number by $Ar = \sqrt{3/4\pi}G$. Recently, Kuznetsov (2015) numerically study the regular and chaotic bahaviors of falling plates using the quasi-steady models introduced by Tanabe & Kaneko (1994), Belmonte *et al.* (1998), Pesavento & Wang (2004), and found two-dimensional descent motion to be rich in dynamics with nonlinear characteristics such as fixed points, limit cycles, attractors, and bifurcations.

Recent experimental studies by Heisinger *et al.* (2014), found probability density functions (*pdf*) associated with the landing distribution for each of the four falling modes. They found that the center is one of the least likely landing site for non-steady descents, characterized by dips in the *pdf* around the center. For tumbling descent, the *pdf* forms a ring structure about the center, while for chaotic descents the *pdf* distribution is much more widely distributed. Vincent *et al.* (2016) later investigate the falling behaviors of annular discs in the same Re and I^* space, and found the central hole in the disc to be a stabilizer of the descent motion as the inner edge forms an counter-rotating vortex ring to that of the outer edge.

This paper investigates the gravitational settling of heavy discs in the presence of stably-stratified salt water as compared to a constant density water background. The final landing location for multiple drops are recorded to compute the landing distribution, where the influence of stratification is documented. To further study the effect of stratification, descent trajectories and orientations are reconstructed for the free-fall fluttering disc. The results presented here may have a direct impact on many environmental and engineering processes where detailed understanding of the descent dynamics in stratified flow is of significant importance.

2. Methods

To investigate how the presence of stratification influence the trajectory descent motion a disc and fluid system is selected, such that, the descent mode does not change after stratification, i.e., the fluttering motion of a disc observed in pure water will persist even after the background fluid is now linearly stratified with salt-water. Although, a transition in the descent mode would be of interests, our initial investigation is to understand the quantitative differences of a disc in free-falling fluttering descent when the fluid is stratified and no longer of constant density.

Due to practical experimental limitations, such as safety and cost, we elected to use salt-water for the stratification process. A two-tank (or double-tank) method is used to generate a stable linear density profile in the main or test tank. This method was proposed by Fortuin (1960) and Oster (1965), where a forced-drained approach applying mechanical pumps to control the fluid flow was used. A summary of the setup and stratification process can be reviewed in Hill (2002). Here we use a free-drained approach, which rely on gravity and not pumps, to produce the linear vertical stratification. To produce a top-filled stable vertical stratification ($\gamma = d\rho/dz < 0$) with the higher density at the bottom and the lower density solution at the top of the tank, two tanks of equal sizes (approximate 1/2 of the main tank) with different density is required. In our case the fluid lower density fluid is water ($\rho_1 \approx 1000\ kg/m^3$) and the higher density is salt-water solution ρ_2. During the tank filling process, the lower density fluid (ρ_1) flows to the higher density (ρ_2) tank where it is mixed prior to filling the main experimental tank. A sponge and floater are used to ensure that the fluid is evenly distributed by minimizing mixing and remains top filled. A schematic showing the setup is shown in figure 1b.

In dealing with non-stratified and stratified effects the time scale τ depends on the physical process. For example, with viscous effects $\tau = L^2/\nu = d^2/\nu$, and, therefore, the time scale is $\mathrm{Re} = \tau/(L/U) = Ud/\nu$ with velocity scale U and length scale $L = d$. For stratification effects, we have $\tau = 1/N$ and the time is $\mathrm{Fr} = \tau/(L/U) = U/Nd$. Therefore, including the dimensionless moment of inertia $I^* = I/\rho_f d^5 = \pi\rho t/64\rho_f d$ described in §1, the three main non-dimensional parameters that govern motion for descending disc are I^*, Re, and Fr. Furthermore, since our investigation deals with descent ranges and heights that are much greater than the disc diameter ($h >> d$), it is occasionally more relevant to scale these lengths by the descent height h instead of the disc diameter d, e.g., reporting descent depth.

To investigate the fluttering motion, an acrylic disc ($\rho = 1143.7\ kg/m^3$) with dimensions $d = 2.54$ cm and $t = 2$ mm (see figure 1a) was selected for the baseline case. In the (Re, I^*) space, this place the motion in the fluttering mode regime with a dimensionless moment of inertia $I^* = 0.0035$ and Reynolds number of $\mathrm{Re} = 1640$. The average speed U is not known *a priori* and is found by experimentally dropping the disc and recording the time it takes to descend the length of the tank. Table 1 lists the key parameters used throughout this paper.

The investigation tank is a cubic acrylic container, 0.61 m on each side (≈ 60 gallons), see figures 2 and 1b. In the experiments, the discs were released with near zero initial conditions just below the surface of the fluid using an electromagnetic release mechanism. To determine the uncertainty inherent in the release mechanism, a heavy disc is released in air 10 times using the release mechanism. The standard deviation of the steel disc descent was within 1.5% of the vertical drop distance.

For the landing distribution, the location of the disc at the bottom of the tank is recorded with a top mounted camera. To prevent the disc from sliding while it lands, a grid mesh was added to to the bottom of the tank. For the reconstruction of the descent

Case	I^*	Re	Fr	Ri	N (rad/s)	U (cm/s)	A (mm/s)
Water	0.0044	1580	∞	0	0	5.60±0.34	-0.23±0.31
Stratified-1	0.0042	1141	1.51	501	1.06	4.04±0.31	0.84±0.40
Stratified-2	0.0041	1094	0.90	1336	1.69	3.88±0.15	0.85±0.16

TABLE 1. Key dimensional and non-dimensional parameters. An average fluid density value was used to compute I^* for the stratified cases. U is the mean descent speed of the disc, and A is the mean z-direction acceleration of the disc.

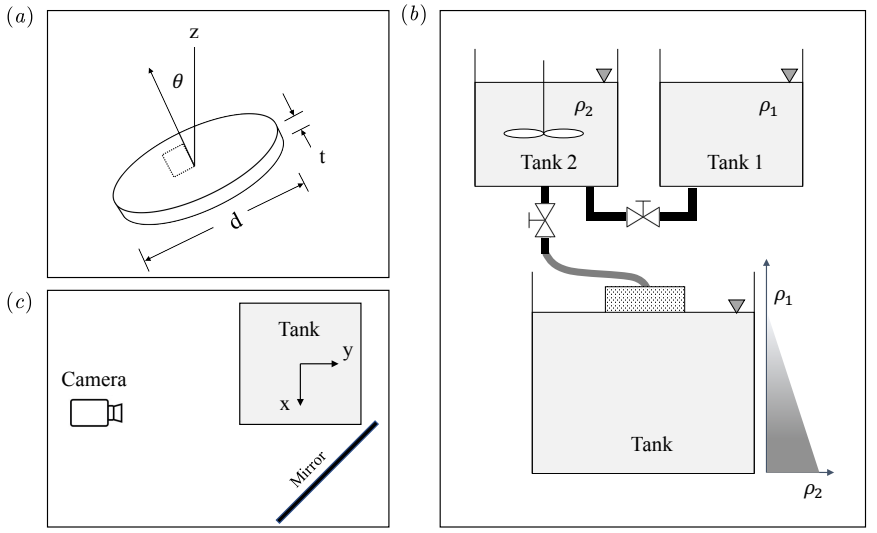

FIGURE 1. (a) Disc schematic, where θ is the angle between the vertical z direction and the disc normal direction. (b) Two-tank experimental free-drained setup used to generate a stable linear density profile in the tank. (c) Top view of the experimental tank and camera setup. A mirror is placed and aligned to obtain the orthogonal side view of the tank needed for the image processing and reconstruction of the disc's trajectory and orientation.

trajectory and orientation, the fluttering descents were recorded using a high resolution digital video camera (Point Grey Grasshopper3) set to a moderate frame rate > 50 fps. The camera and tank setup is shown in figure 1c. To obtain the corresponding side view of the disc's descent, a mirror is used. Proper calibration is required to adjust for the mirrored view. The position and orientation are obtained directly from the reconstructed trajectory after high frequency noise are removed. The velocity and orientation rates were obtained using finite differencing. The experimental setup and procedure, including the image processing algorithm for the trajectory and orientation reconstructions, are similar to those of Heisinger *et al.* (2014) and Vincent *et al.* (2016). The overall process and experiment is depicted in figure 2.

3. Landing Distribution

To test the influence stratification has on the disc's trajectory in the fluttering regime we use pure water as our baseline for the disc and tank described in §2. Drops are made in water and near identical drops are made in the stratified flow. Repeating the experiment

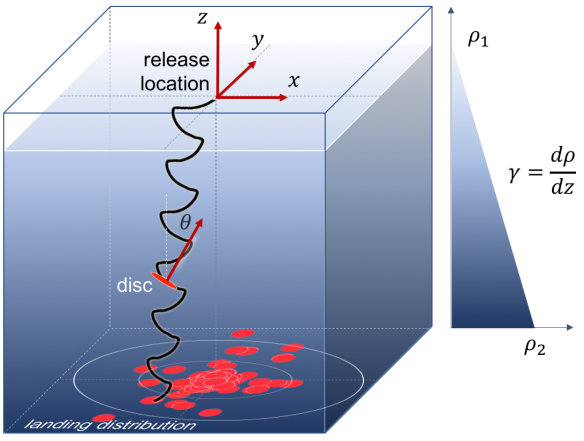

FIGURE 2. (Colour online) Schematic of the tank setup with the coordinate system centered at the initial release location. An example of a reconstructed trajectory is shown. The final landing location for multiple drops are recorded to compute the landing distribution.

done by Heisinger *et al.* (2014), we made multiple repeated drops ($n = 500$) in pure water initially centered at $(0, 0)$ to obtain our baseline for the fluttering case. The resulting landing distribution for the drops in water, expressed as histogram of probability per unit bin, is shown in figure 3a, and the radial distribution is shown in figure 3c. Our results are similar to those by Heisinger *et al.* (2014), where a dip in the radial histogram near the origin and a tight radial distribution (standard deviation $\sigma < 10\%$ descent height) are observed.

To observe the influence stratification has on the radial distribution we repeat the ($n = 500$) drops in stratified flow with Fr $= 0.9$ (density gradient $\gamma = -290 kg/m^4$). Figure 3b shows the distribution of the landing location for stratified flow case; when compared to figure 3a, we note a larger radial dispersion. Assuming normal distribution profiles, the ratio of the mean standard deviations of the final landing distribution for descents in stratified flow to that of water is $\langle\sigma\rangle_s / \langle\sigma\rangle_w = 1.92$. This larger radial distribution is more evident in figure 3c, which shows the histogram of the radial distributions for both water and stratified flow. Assuming a lognormal probability density function, the variance for the descents are $r^w_\nu = 0.002$ for water and $r^s_\nu = 0.011$ for stratified flow, or $\sqrt{r^s_\nu / r^w_\nu} = 2.35$. The differences in the mean is $r^w_m = 0.06$ for water and $r^s_m = 0.084$ for stratified flow, or $r^s_m / r^w_m = 1.4$. Observing the cumulative distribution function (cdf) in figure 3d, we observe that two curves deviate quickly after $r/h > 0.05$. At $r/h = 0.11$, 90% of the drops in water are accounted. For the stratified case, the 90% cumulation is reached at $r/h = 0.20$. A summary of the distribution parameters are listed in table 2. In general, a larger landing dispersion is observed for descents in stratified flow.

4. Trajectory Reconstruction

The analysis of the landing sites of descending discs provide insight on how stratification influence the radial dispersion. However, it provides no temporal and state information of the descent motion. From visual inspection of the descents with the naked eye we see something similar to figure 4, where the following qualitatively differences can be observed: descents in stratified flow have larger landing dispersion (which was

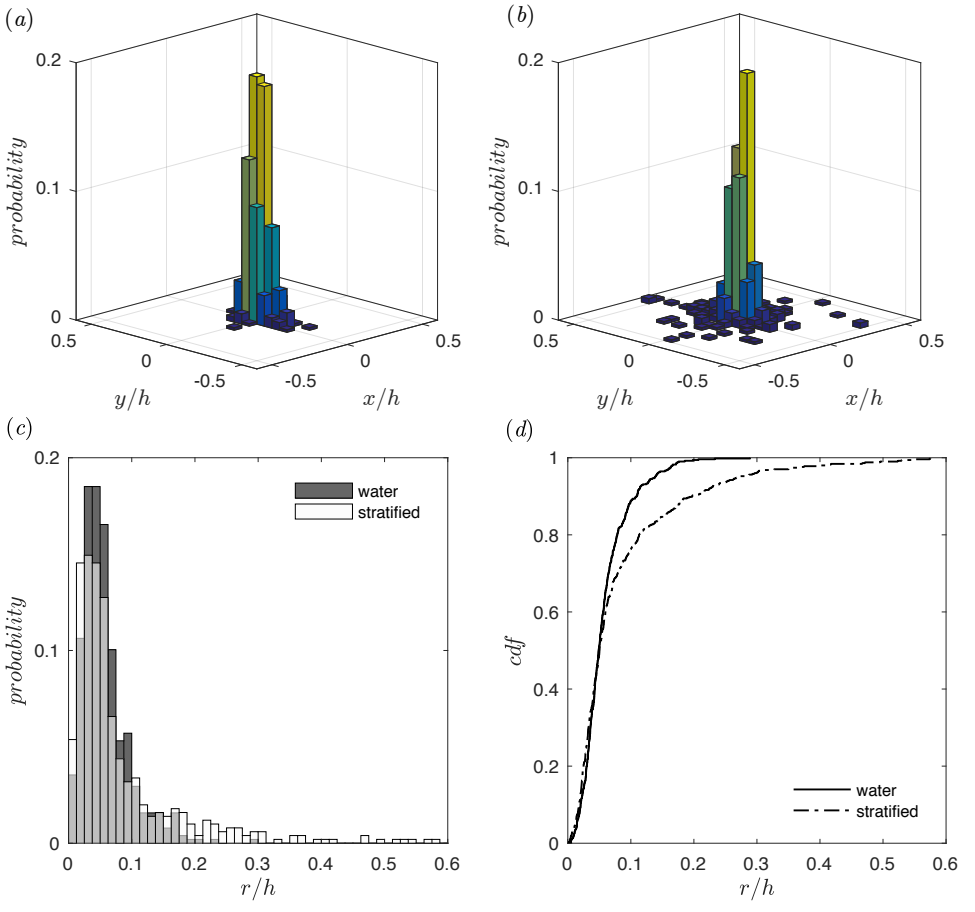

FIGURE 3. (Colour online) Distribution of the final landing location, expre ssed in probability per bin, for 500 free-fall fluttering discs in (a) water and (b) stratified flow (Fr = 0.9), initially released from $(x, y) = (0,0)$. (c) Histogram of the range distribution. (d) The cumulative distribution function (*cdf*). x, y, and r are normalized by the fluid depth, h.

Case	Fr	σ_1/h	σ_2/h	r_m/h	r_{var}/h	0.9 *cdf*
Water	∞	0.055	0.036	0.060	0.002	$r/h = 0.11$
Stratified	0.9	0.097	0.078	0.084	0.011	$r/h = 0.20$

TABLE 2. Distribution parameters of the final landing distribution. σ_1 and σ_2 are the standard deviations along the major and minor axes from figure 3a-b. r_m and r_{var} are the mean and variance of the radial distribution normalize by the descent height h, and *cdf* is the cumulative distribution function as shown in figure 3d.

quantified in the previous section) and longer descent time. It is noted that this larger dispersion is not due to the increase in the fluttering amplitude (side-to-side distance), which decreases, but is due to the drift in the mean radial distances.

As an example, figure 5 shows two reconstructed fluttering descents released from rest, one in pure water and another in Fr = 0.90 stratified fluid. Snap shots views at different time intervals are shown for both cases 5, where the viewing angle have been maximized

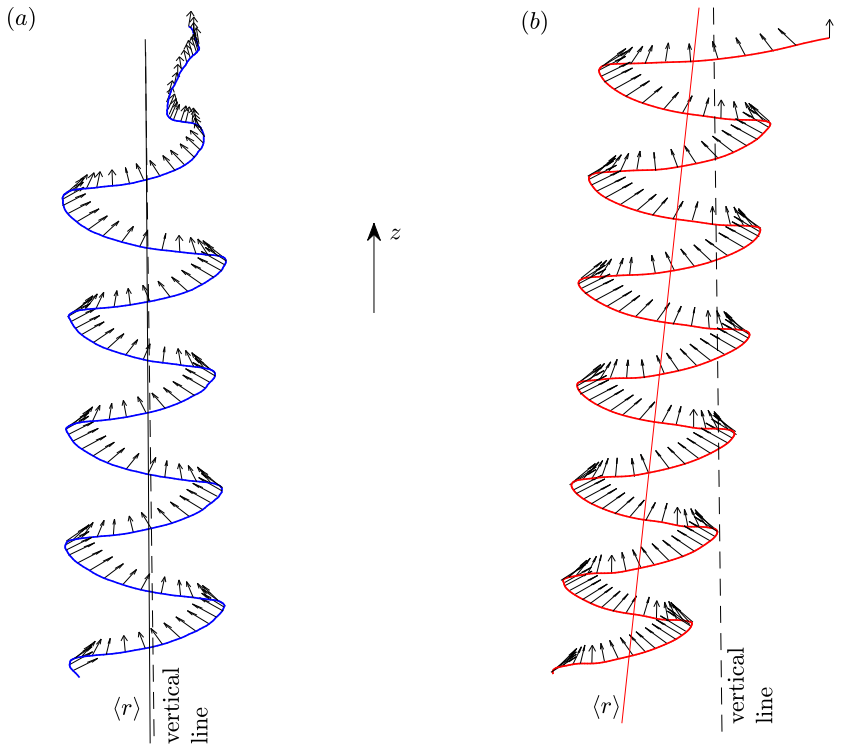

FIGURE 4. An example of a descent in (a) water and (b) stratified flow depicting the qualitative observed differences: enhance radial drift of the mean range $\langle r \rangle$ from vertical line, and decrease fluttering amplitudes in stratified flow. Arrows are the direction normal to the disc.

to show as much of the fluttering motion as possible. The time interval was selected to show approximately 1 cycle of the fluttering motion. During the descent the disc can gyrate and the fluttering motion can no longer be observed in certain angles, as shown in the water example. From figure 5, we note two clear observations regarding the two cases: (1) for one cycle, the water descents duration are about 1.3 seconds for both the cycle near the top and near the bottom, and descending about 3.2 D (disc's diameter) each cycle, or roughly at 2.5 D/sec. (2) For the stratified flow, we note that near the begining of the descent that descent time for one cycle is approximately 1.4 seconds covering about 2.5 D, and the near the bottom the stratified descent is covering about 2.5 D in 1.6 seconds, or roughly a decrease in speed from 1.8 D/sec to 1.6 D/sec between the two cycles. This observation is consistent with intuition, since the density of the stratified fluid is increasing with depth we expect the drag to increase proportionally, thus, decelerating the descending disc and increase the descent time.

To investigate further, trajectories are reconstructed in water and stratified flow, at Fr = 1.51 (N = 1.06 rad/s) and Fr = 0.90 (N = 1.69 rad/s), with focus on the latter. The discs are released with near zero initial conditions top center of the tank, with the x-axis along the front of the tank (left-to-right), y-axis along the depth of the tank, and z-axis along the height of the tank centered at the initial drop location, as illustrated in figure 2. Coin descents are recorded and processed as described in §2 for reconstructing the position and orientation information.

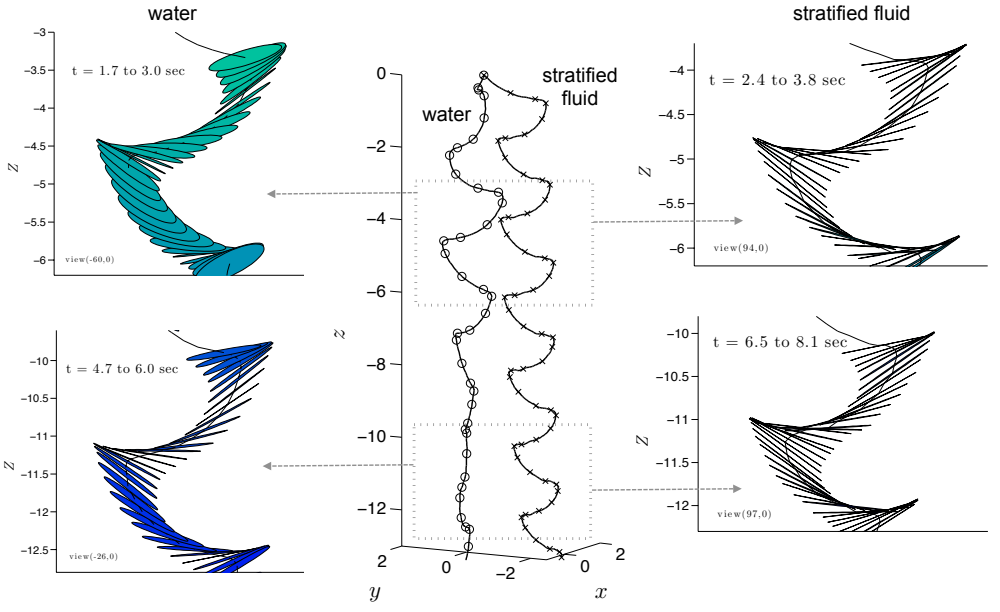

FIGURE 5. Example reconstructed fluttering motion in water (○) and stratified flow (x) with snap shots views showing the fluttering motion and orientation at different time intervals. View angles of the snap shots inserts are orientated to maximize observation of the fluttering motion.

4.1. *Effect of Stratification on Horizontal Motion*

As mentioned above descents in stratified flow were observed to have larger landing dispersion, and that dispersion is due to a drift of the mean descent motion and not due to an increase in the fluttering amplitude. The former can be seen by reconstructing the motion for 10 descents in water and 10 descents in Fr = 0.9 stratified flow. After removing the first cycle of the flutter to account for any transient behaviors, we can observe the drift by plotting the mean range of a fluttering arc (between inflection points) versus the mean range of the next flutter arc (as shown in figure 6). If there is no drift in the mean radial range the points should stay near $(0, 0)$, as shown in figure 6a, which are the reconstruction cases for descents in water. The mean distances from $(0, 0)$ for descent cases in water is 0.075 ± 0.095. For the descent cases in stratified flow, we note many more cases show drifts in the mean arc ranges (figure 6b), where the mean distances from $(0, 0)$ is 0.174 ± 0.150. Although, the no-drift versus drift behaviors are not exclusive to descents in water and stratified flow, respectively, the figure does show that the mean descent motion in stratified flow tend to drift more frequently than that of pure water descents. A behavior which explains why we see larger landing dispersion for descents in stratified flow in §3.

The decrease in the fluttering amplitude in stratified flow can be observed in figure **??**.

4.2. *Effect of Stratification on Vertical Motion*

A pronounced result of stratification is the affect it has on the vertical descent motion, z. Figure 7 shows the vertical descent motion z and $\dot{z}$, where z is normalized by the depth of the fluid h, and $\dot{z}$ is normalized by the mean descent speed in pure water (see table 1). Here we note the difference in the descent time. In the pure water fluid, the

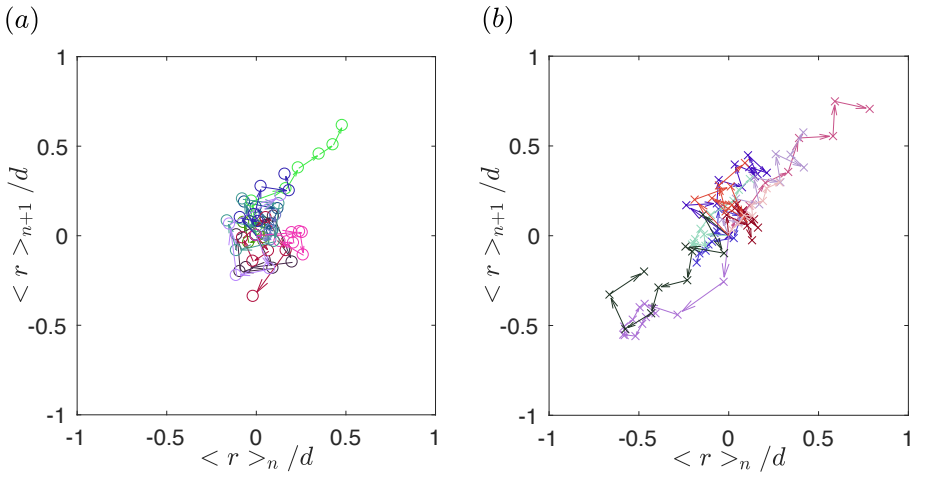

FIGURE 6. (Colour online) Phase plot showing reconstructed mean range of the n-th fluttering arc versus the $n+1$ arc for descents in (a) water and (b) Fr $= 0.9$ stratified fluid. Ranges are normalized by the disc diameter d. An arc is from one inflection point to another inflection point in the flutter motion. Initial point centered at $(0, 0)$. Varying colors for different descent cases.

average disc descent times is approximately $T_w = 6.5$ sec, while the cases in stratified fluid are nearing $T_w = 10$ sec to descend, or $T_s/T_w = 1.54$. In addition to the descent duration, the slope of z as a function of time is no longer linear for the cases in stratified flow, indicating a deceleration in speed as it descends. This descent profile is similar to the descent sediment in stratified flow shown in Blanchette & Bush (2005). Therefore, in this paper the metric used to compare the influence stratification has on the vertical motion is the descent speed $\dot{z}$ and changes in the descent speed $\ddot{z}$.

This deceleration is clearly seen in figure 7b−c, where the descent speed as a function of time and the average descent speed as a function of depth are shown, respectively. To focus only of the fully developed fluttering descent motion, the first few cycles of the transient behavior were removed in figure 7c. Looking at the average descent speed, the descents in water remain steady ($\langle \dot{z} \rangle / U_w = -1 \pm 0.06$) with a small negative slope (linear fit of -0.055), indicating that a terminal speed has not been reached and that the disc continues to speed up as it descends. For the descents in stratified fluid the average descent speed approaches $\langle \dot{z} \rangle / U_w = -0.69 \pm 0.03$, with upward slope or acceleration (in the opposite direction of the motion) of 0.169 (linear fit) exist, indicating the disc is slowing down as it descends.

It is noted, that the vertical descent motion in figure 7 follows closely to the dynamics of a simple descending particle of the form

$$\ddot{z} = -g + \frac{1}{m}\rho_f(z)\, V g + \frac{1}{2m}\rho_f(z)\, |\dot{z}|^2 C_D S \tag{4.1}$$

where $g = 9.806\ m/s^2$, V is the volume of the disc, C_D is the drag coefficient, area $S = \pi d^2/4$, m is the mass, $\rho_f(z) = \rho_0 + \gamma z$, and density gradient $\gamma = d\rho/dz$. The z and $\dot{z}$ state from the dynamical model is overlaid in figure 7 for $C_D = 1.44$ for water descents and $C_D = 1.97$ for stratified flow, where the value of C_D was estimated to best fit to the average reconstructed z state from the experimental data. In both figures, we

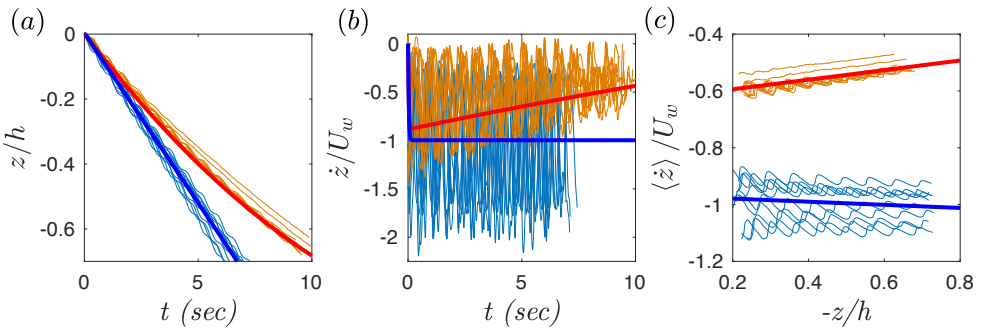

FIGURE 7. (Colour online) (*a*) Descent depth z, (*b*) descent velocity $\dot{z}$ as a function of time, and (*c*) average descent velocity as a function of $-z/h$ for free fall fluttering discs in water (blue) and Fr = 0.9 stratified flow (orange), where z is normalized by the depth of the fluid, h, and $\dot{z}$ is normalized by the mean descent speed in water. Numerically integrated states using (4.2) are overlaid in bold lines for $C_D = 1.44$ for a modeled water descent (blue) and $C_D = 1.97$ for a stratified flow (red) case, where the C_D were selected that best fitted the average reconstructed z state data. In (*c*) linear polynomial fits to the mean experimental data are overlaid for descents in water (blue) and stratified flow (red).

note acceptable agreements for predicting the vertical motion if the drag coefficients are allowed to differ.

The C_D for stratified flow is larger than that of water, $C_D^s/C_D^w = 1.37$. This increase or enhanced drag has also been observed by Torres *et al.* (2000) and Yick *et al.* (2009) for vertical motion of spheres in stratified flow, where they found correlations between C_D and the Froude number Fr, and was investigated further by Doostmohammadi *et al.* (2014). This approximate 30% increase in the drag coefficient has a major implication on modeling and prediction of the trajectory in stratified flow, where the data suggest that there is a shift in the *a priori* mean drag coefficient value. This enhance drag can also be interpreted as an increase in the timing error in a descent model, if the nominal drag coefficient is not corrected.

4.3. *Effect of Stratification on Orientational Motion*

As the discs descends in the fluttering mode, the inclination (angle between the norm vector of the coin and z-axis) will oscillate between extremas as it cycles from maximum inclination to zero inclination to minimal inclination and back to zero inclination. This inclination frequency has been observed to be 1.63 Hz for the average reconstructed descent cases in water and 1.44 Hz for the descents in Fr = 0.9 stratified flow. In figure 8a the peak inclination angle (the maximum angle between the norm vector of the coin and z-axis at the inflection point where the angular rate is near zero) is plotted for ten descents in water (−) and the ten descents in stratified fluid (−).

From figure 8a, a notable decrease in the peak inclination is shown for the stratified cases such that the mean peak inclination ratio is $\langle\theta_p\rangle_s / \langle\theta_p\rangle_w = 0.84$ and a large ratio when comparing the slopes to the mean peak inclination $\left\langle\dot{\theta}_p\right\rangle_s / \left\langle\dot{\theta}_p\right\rangle_w = -9.4$ is found due to the fact that $\left\langle\dot{\theta}_p\right\rangle_w$ is near zero. We believe this decease in inclination rate in the stratified fluid is due to a small restoring torque that exist between the center of gravity and the center of buoyancy. When the inclination angle is non-zero the side of the coin closer to the bottom of the tank will experience higher buoyancy force due to its higher density, thus, causing a torque in the direction which minimizes the inclination angle.

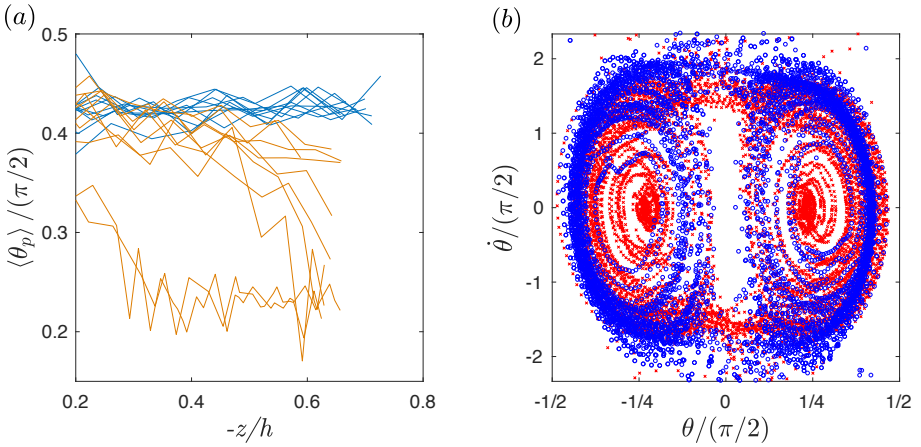

FIGURE 8. (Colour online) (a) peak inclination (maximum inclination angle at the inflection point where the angular rate is near zero) as a function of depth ($-z$), where $-z$ is normalized by the depth of the fluid, h. Cases in water (blue) and Fr = 0.9 stratified fluid (orange). (b) θ-$\dot{\theta}$ phase plot for fluttering descents in water ($\circ$) and Fr = 0.9 stratified fluid (x).

Assuming a hydrostatic model under pure rotation, the restoring angular acceleration due to buoyancy is found to be

$$\ddot{\theta} = -\frac{\rho_0}{2\rho} N^2 \sin(2\theta) \tag{4.2}$$

where ρ_0 is the reference density of the fluid, ρ is the density of the disc, N is the Brunt-Väisälä freqency, and θ is the inclination or nutation angle. The equation is derived by finding the torque on the disc from the offset between the gravitational and buoyancy forces. See §A for the derivation. As an example, for $N = 1.69\ rad/s$, equation 4.3 gives a maximum radial restoring acceleration of $2.49\ rad/s^2$ at $\theta = \pm\pi/4$, and zero at $\theta = 0$ (when the disc is parallel to the horizontal plane) and $\theta = \pm\pi/2$ (when the disc is perpendicular to the horizontal plane). Equation 4.3 provides a non-linear relation with θ, that is similar to the motion of pendulum. We also note, that equation 4.3 also requires that $\left|\ddot{\theta}\right| \leqslant \frac{\rho_0}{2\rho} N^2$. Therefore, for heavy objects, where the disc density $\rho \gg \rho_0$, we have $\left|\ddot{\theta}\right| \approx 0$. If the descending disc is near the density of the fluid, $\rho \approx \rho_0$, we have, $\left|\ddot{\theta}\right| \leqslant N^2/2$.

From experimental data (figure 8b), we do not always observe such behavior for fluttering descents with or without stratification. Instead it appears that for some cases, the librating region occurs away from $\theta = 0$ in pairs, yet still bounded to $\theta_{max} \approx \pm\pi/4$. The result is consistent with our understanding of disc dynamics for non-steady descents, where a disc released with zero initial inclination would begin to rotate and the disc would eventually either flutter, tumble, or a chaotic combination of fluttering and tumbling. Furthermore, these librating regions around the $\theta \approx \pm\pi/8$ fixed points, corresponds to hula-hoop descents (Auguste *et al.* 2013), where the inclination angle never goes to zero, but precess with a near constant angle. Note that, although the inclination angle is taken always to be positive, by definition, in selected analysis it is useful to define a moving plane to view orientation changes comparable to experiments and computations done in two dimensions, as with figure 8b.

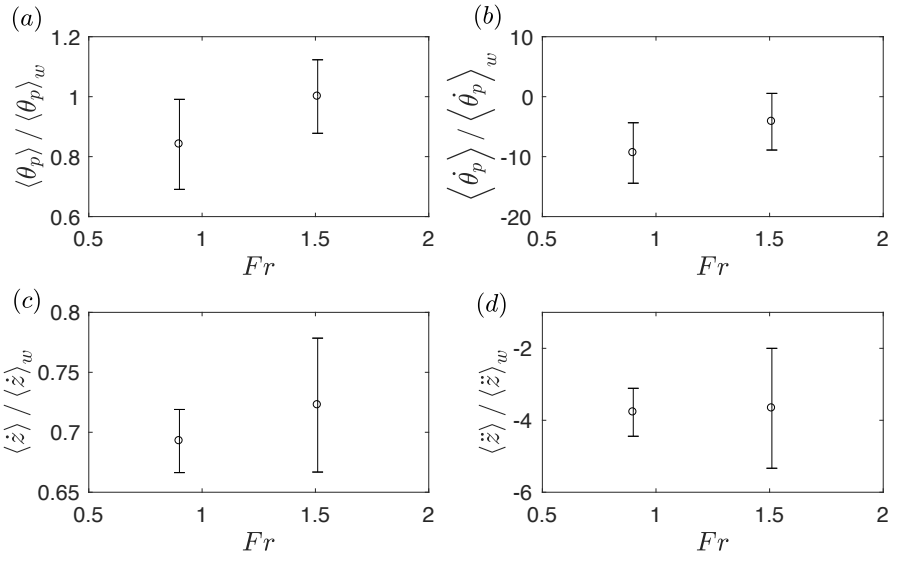

FIGURE 9. Average (a) peak inclination, (b) peak inclination rate, (c) vertical speed, and (d) vertical acceleration, for ten reconstructed descents in stratified flow as compared to descents in water. Error bars are 1σ standard deviations.

Fr	$\langle\theta_p\rangle \,/\, \langle\theta_p\rangle_w$	$\left\langle\dot{\theta}_p\right\rangle \,/\, \left\langle\dot{\theta}_p\right\rangle_w$	$\langle\dot{z}\rangle \,/\, \langle\dot{z}\rangle_w$	$\langle\ddot{z}\rangle \,/\, \langle\ddot{z}\rangle_w$
1.51	1.00 ±0.12	-4.18 ±4.74	0.72±0.06	-3.58±1.68
0.90	0.84 ±0.15	-9.41 ±5.05	0.69±0.03	-3.66±0.70

TABLE 3. Average reconstructed results for fluttering descents for salt-stratified flow as compared to water descents, where θ_p is the peak inclination, $\dot{\theta}_p$ is the rate of the peak inclination, $\dot{z}$ is the descent speed, $\ddot{z}$ is the rate of the descent speed. Errors are 1σ standard deviations from ten reconstructed cases.

Reconstructed results between descents in water and descents in stratified flows are summarized in figure 9 and in table 3, including the results from the Fr = 1.51 ($N = 1.07\ rad/s$) stratified flow cases.

5. Conclusion

Descent motion of discs and cards have warranted a lot of attention in the recent decades, both experimentally and numerically (see, for example, Ern *et al.* (2012) and Kuznetsov (2015)). The motion of these free falling objects are generally complex as the solid body and the fluid interacts affecting the path of the falling object. However, for small thickness-to-width ratio the general descent behavior (steady, fluttering, tumbling, or chaotic) can be determined based on the Reynolds number, Re, and the dimensionless moment of inertia, I^* (see Field *et al.* (1997)).

This paper investigated the affect stable vertical stratification has on the fluttering falling motion of discs. By dropping multiple discs with similar initial conditions and reconstructing their states, we found that stratification enhances the radial dispersion of the disc ($\sigma_{N=1.69}/\sigma_{N=0} \approx 2$), while simultaneously, decreasing the vertical descent speed

and the inclination angle during the descent. Similar enhanced drag observed by Torres *et al.* (2000), Yick *et al.* (2009), and Doostmohammadi *et al.* (2014) for vertical motion are observed here. We note, that wider landing dispersions is usually associated with chaotic descent motion (a combination of fluttering and tumbling) in the pure water case, as shown in Heisinger *et al.* (2014). However, stratification appears to perform similar, albeit smaller, enhancing of the absolute radial motion without tumbling, thus, the discs never flips. This increase in spacial and temporal errors, suggests that stratification can become a major error source in modeling and predicting descent motion in stratified flow.

The understanding of disc distribution due to stratification effects may have a significant impact on the understanding of unpowered robotic descents, and geological and biological transport, where density and temperature variations may occur. We can imagine engineering applications where such behavior could be useful, for example, placement of photonic solar cells on micro robotics where landing distribution is to be maximized (see Valdes *et al.* 2012; Pounds *et al.* 2016), or enhance our understanding of accidental drops of objects such as pipes during offshore operations (see Yasseri 2014; Majed *et al.* 2013; Awotahegn *et al.* 2016).

Acknowledgements

This work is partially supported by the NSF grant CMMI 13-63404. The authors would like to also thank Stephen Rolfe and Joe Frigo for their assistances with the experiments.

Appendix A

The restoring angular acceleration due to buoyancy for a hydrostatic model is found by first computing the buoyancy offset due to the stratification by integrating the buoyancy element over the disc's volume, then

$$x_B = \frac{\int_V x\rho \, \partial V}{\rho_0 V} \tag{A 1}$$

where $\rho = \rho_0 - |\gamma| x \sin(\theta)$, γ linear fluid density gradient, ρ_0 is the fluid density at the center of the disc, x is the direction along the line of the buoyancy offset centered at the disc, and θ is the inclination angle between the disc's plane and the horizontal plane. In the body centered coordinate system, z is the axis of rotation of the disc, and y normal to the disc plain and completing the right-hand rule. Assuming a cylindrical disc of thickness t and diameter D, the integration yields

$$x_B = -\frac{|\gamma| D^2}{16\rho_0} \sin(\theta). \tag{A 2}$$

The torque due to the buoyancy offset for a pure inclination rotation is then

$$\begin{aligned} \tau_B &= \rho_0 g V x_B \cos(\theta) \\ &= -\frac{1}{16} g V D^2 |\gamma| \sin(\theta)\cos(\theta). \end{aligned} \tag{A 3}$$

Similarly, the angular acceleration due to buoyancy for a pure inclination rotation for a homogenous solid disc of density ρ_{disc} is found to be

$$\begin{aligned}\ddot{\theta} &= -\frac{\rho_0 N^2 V D^2}{16 I}\sin(\theta)\cos(\theta) \\ &= -\frac{\rho_0}{2\rho}N^2 \sin(2\theta) \end{aligned} \tag{A 4}$$

where ρ_0 is the density of the fluid at the disc's center, ρ is the density of the disc, N is the Brunt-Väisälä frequency, and θ is the inclination or nutation angle.

REFERENCES

Andersen, Anders, Pesavento, Umberto & Wang, Z Jane 2005*a* Analysis of transitions between fluttering, tumbling and steady descent of falling cards. *Journal of Fluid Mechanics* **541**, 91–104.

Andersen, A, Pesavento, U & Wang, Z Jane 2005*b* Unsteady aerodynamics of fluttering and tumbling plates. *Journal of Fluid Mechanics* **541**, 65–90.

Auguste, Franck, Magnaudet, Jacques & Fabre, David 2013 Falling styles of disks. *Journal of Fluid Mechanics* **719**, 388–405.

Awotahegn, Michael Berhe, Oosterkamp, Ljiljana Djapic, Nystrøm, Per Richard & others 2016 3d study of dropped object motion in sea water based on scale test. In *The 26th International Ocean and Polar Engineering Conference*. International Society of Offshore and Polar Engineers.

Belmonte, Andrew, Eisenberg, Hagai & Moses, Elisha 1998 From flutter to tumble: inertial drag and froude similarity in falling paper. *Physical Review Letters* **81** (2), 345.

Blanchette, François & Bush, John WM 2005 Particle concentration evolution and sedimentation-induced instabilities in a stably stratified environment. *Physics of Fluids* **17** (7), 073302.

Chrust, Marcin, Bouchet, Gilles & Duek, Jan 2013 Numerical simulation of the dynamics of freely falling discs. *Physics of Fluids* **25** (4).

Doostmohammadi, A, Dabiri, S & Ardekani, AM 2014 A numerical study of the dynamics of a particle settling at moderate reynolds numbers in a linearly stratified fluid. *Journal of Fluid Mechanics* **750**, 5–32.

Ern, Patricia, Risso, Frédéric, Fabre, David & Magnaudet, Jacques 2012 Wake-induced oscillatory paths of bodies freely rising or falling in fluids. *Annual Review of Fluid Mechanics* **44**, 97–121.

Field, Stuart B, Klaus, M, Moore, MG & Nori, Franco 1997 Chaotic dynamics of falling disks. *Nature* **388** (6639), 252–254.

Fortuin, JMH 1960 Theory and application of two supplementary methods of constructing density gradient columns. *Journal of Polymer Science* **44** (144), 505–515.

Ganzevles, Sander PM, van Nuland, Fons SW, Maas, Leo RM & Toussaint, Huub M 2009 Swimming obstructed by dead-water. *Naturwissenschaften* **96** (4), 449–456.

Heisinger, Luke, Newton, Paul & Kanso, Eva 2014 Coins falling in water. *Journal of Fluid Mechanics* **742**, 243–253.

Hill, DF 2002 General density gradients in general domains: the two-tank method revisited. *Experiments in fluids* **32** (4), 434–440.

Jin, Changqiu & Xu, Kun 2008 Numerical study of the unsteady aerodynamics of freely falling plates. *Comm. Comp. Phys* **3**, 834–851.

Kuznetsov, Sergey P 2015 Plate falling in a fluid: Regular and chaotic dynamics of finite-dimensional models. *Regular and Chaotic Dynamics* **20** (3), 345–382.

Lee, Cunbiao, Su, Zhuang, Zhong, Hongjie, Chen, Shiyi, Zhou, Mingde & Wu, Jiezhi 2013 Experimental investigation of freely falling thin disks. part 2. transition of three-dimensional motion from zigzag to spiral. *Journal of Fluid Mechanics* **732**, 77–104.

Lin, EIH 1982 Nasa-cr-168635: A review of the salt-gradient solar pond technology .

Lofquist, Karl EB & Purtell, L Patrick 1984 Drag on a sphere moving horizontally through a stratified liquid. *Journal of Fluid Mechanics* **148**, 271–284.

Maas, LRM & van Haren, H 2006 Worden mooi-weer verdrinkingen door dood-water veroorzaakt. *Meteorologica* **15**, 211–216.

MacIntyre, Sally, Romero, José R, Silsbe, Gregory M & Emery, Brian M 2014 Stratification and horizontal exchange in lake victoria, east africa. *Limnology and Oceanography* **59** (6), 1805–1838.

Majed, Arya, Cooper, Phil & others 2013 High fidelity sink trajectory nonlinear simulations for dropped subsea objects. In *The Twenty-third International Offshore and Polar Engineering Conference*. International Society of Offshore and Polar Engineers.

Maxwell, James Clerk 1990 *The Scientific Letters and Papers of James Clerk Maxwell: 1846-1862*. CUP Archive.

Mercier, Matthieu, Vasseur, Romain & Dauxois, Thierry 2011 Resurrecting dead-water phenomenon. *arXiv preprint arXiv:1103.0903* .

Oster, Gerald 1965 Density gradients. *Scientific American* **213**, 70–76.

Pesavento, Umberto & Wang, Z Jane 2004 Falling paper: Navier-stokes solutions, model of fluid forces, and center of mass elevation. *Physical review letters* **93** (14), 144501.

Pounds, Paul, Potie, Timothy, Kendoul, Farid, Singh, Surya, Jurdak, Raja & Roberts, Jonathan 2016 Automatic distribution of disposable self-deploying sensor modules. In *Experimental Robotics*, pp. 535–543. Springer.

Stringham, GE, Simons, Daryl B & Guy, Harold P 1969 *The behavior of large particles falling in quiescent liquids*. US Government Printing Office.

Tanabe, Yoshihiro & Kaneko, Kunihiko 1994 Behavior of a falling paper. *Physical Review Letters* **73** (10), 1372.

Torres, CR, Hanazaki, H, Ochoa, J, Castillo, J & Van Woert, M 2000 Flow past a sphere moving vertically in a stratified diffusive fluid. *Journal of Fluid Mechanics* **417**, 211–236.

Torres, Carlos R, Ochoa, José, Castillo, JoséE & Hanazaki, Hideshi 1999 Numerical simulation of flow past a sphere in vertical motion within a stratified fluid. *Journal of computational and applied mathematics* **103** (1), 67–76.

Valdes, Samuel, Urza, Ignacio, Pounds, Paul & Singh, Surya 2012 Samara: low-cost deployment for environmental sensing using passive autorotation. In *Robotics: Science and Systems Workshop on Robotics for Environmental Monitoring*. Citeseer.

Vincent, Lionel, Shambaugh, W Scott & Kanso, Eva 2016 Holes stabilize freely falling coins. *Journal of Fluid Mechanics* **801**, 250–259.

Willmarth, William W, Hawk, Norman E & Harvey, Robert L 1964 Steady and unsteady motions and wakes of freely falling disks .

Yasseri, Sirous 2014 Experiment of free-falling cylinders in water. *Underwater Technology* **32** (3), 177–191.

Yick, King Yeung, Torres, Carlos R, Peacock, Thomas & Stocker, Roman 2009 Enhanced drag of a sphere settling in a stratified fluid at small reynolds numbers. *Journal of Fluid mechanics* **632**, 49–68.

Zhao, Haihua & Peterson, Per F 2010 An overview of modeling methods for thermal mixing and stratification in large enclosures for reactor safety analysis. In *The 8th International Topical Meeting on Nuclear Thermal-Hydraulics, Operation and Safety (NUTHOS-8). Shanghai*.

Zhong, Hongjie, Lee, Cunbiao, Su, Zhuang, Chen, Shiyi, Zhou, Mingde & Wu, Jiezhi 2013 Experimental investigation of freely falling thin disks. part 1. the flow structures and reynolds number effects on the zigzag motion. *Journal of Fluid Mechanics* **716**, 228–250.